Mon. Not. R. Astron. Soc. **357,** 599–607 (2005) doi:10.1111/j.1365-2966.2005.08661.x

Fe XXV and Fe XXVI lines from low-velocity, photoionized gas in the X-ray spectra of active galactic nuclei

Stefano Bianchi,[1⋆] Giorgio Matt,[1] Fabrizio Nicastro,[2] Delphine Porquet[3] and Jacques Dubau[4]

[1]*Dipartimento di Fisica, Università degli Studi Roma Tre, Via della Vasca Navale 84, I-00146 Roma, Italy*
[2]*Harvard-Smithsonian Center for Astrophysics, 60 Garden Street, Cambridge, MA 02138, USA*
[3]*Max-Planck-Institut für extraterrestrische Physik, Postfach 1312, 85741 Garching, Germany*
[4]*Laboratoire d'Interaction du rayonnement X Avec la Matière, Université Paris-Sud, 91405 Orsay cedex, France*

Accepted 2004 November 22. Received 2004 November 22; in original form 2004 September 9

ABSTRACT

We have calculated the equivalent widths of the absorption lines produced by Fe XXV and Fe XXVI in a Compton-thin, low-velocity photoionized material illuminated by the nuclear continuum in active galactic nuclei. The results, plotted against the ionization parameter and the column density of the gas, are a complement to those presented by Bianchi & Matt for the emission lines from the same ionic species. As an extension to the work by Bianchi & Matt, we also present a qualitative discussion on the different contributions to the He-like iron emission line complex in the regimes where recombination or resonant scattering dominates, providing a useful diagnostic tool to measure the column density of the gas. Future high-resolution missions (e.g. *Astro-E2*) will allow us to fully take advantage of these plasma diagnostics. In the meantime, we compare our results with an up-to-date list of Compton-thick and unobscured (at least at the iron line energy) Seyfert galaxies with emission and/or absorption lines from H- and He-like iron observed with *Chandra* and *XMM–Newton*.

Key words: line: formation – galaxies: Seyfert – X-rays: galaxies.

1 INTRODUCTION

The present generation of X-ray missions, *XMM–Newton* and *Chandra*, are revealing new features in the spectra of active galactic nuclei (AGN). An interesting case is represented by the observation of emission lines from Fe XXV and Fe XXVI in unobscured Seyfert galaxies (see e.g. Bianchi et al. 2004, for the incidence of these features in a sample of bright objects). Bianchi & Matt (2002) have shown that these narrow lines can share a common origin with those more commonly found in obscured objects, likely produced in a Compton-thin, photoionized material illuminated by the nuclear continuum (see e.g. Matt et al. 2004b, for one of the best-studied examples, NGC 1068).

This interpretation is in agreement with orientation-based unification models of AGN (like the archetypal one introduced by Antonucci 1993). Indeed, the same photoionized material should be present in both obscured and unobscured objects, the only difference being that in the latter its presence is more difficult to observe because the lines are diluted by the nuclear continuum.

Another piece of information was added to this scenario very recently, with the detection of ionized iron lines also in absorption. Though in some cases the line energies are so blueshifted to imply high-velocity outflows (e.g. Reeves, O 'Brien & Ward 2003; Pounds et al. 2003, and references therein), there is now significant evidence of Fe XXV absorption lines occurring in material with low velocity with respect to the rest frame of the source (Kaspi et al. 2002; Matt et al. 2004a; Vaughan & Fabian 2004; Reeves et al. 2004). In the latter situation, the photoionized matter is likely the same revealed in emission in other objects but observed along the line of sight.

The plots of Bianchi & Matt (2002) were produced by summing up all the transitions of a given ion. Although this is a good approximation for such weak emission lines when observed with the CCD resolution of the instruments aboard *XMM–Newton* or the limited effective area available at the iron energy with *Chandra* High Energy Transmission Grating Spectrometer (HETGS) (but see below for some possible diagnostics even in these cases), it will be no longer sufficient with future, high-energy resolution missions, such as *Astro-E2*. With an energy resolution of 6 eV (FWHM) and an effective area of 150 cm^{-2} at 6 keV, the calorimeters aboard *Astro-E2* will be capable of resolving both the Fe XXVI Kα doublet and the w, x, y and z lines from Fe XXV.

In this paper, we investigate the properties of the photoionized material as observed through absorption and emission features from Fe XXV and Fe XXVI. Following the approach by Bianchi & Matt (2002) for the emission lines, we calculate the equivalent

⋆E-mail: Stefano.Bianchi@sciops.esa.int

Table 1. The adopted parameters for the theoretical models developed in this paper (see text for details). All line parameters are taken from the NIST Atomic Data base (http://physics.nist.gov/cgi-bin/AtData/main_asd and references therein), if not otherwise stated.

Continuum						
Table power law Γ				2.0		
n_e				10^6 cm^{-3}		
T				10^6 K		
A_{Fe}				4.68×10^{-5} [a]		
Ion	E_m [b] (keV)	Line Id.	E (keV)	f_{lu}	g_i	g_k
Fe XXV	6.697	Kα w (r)	6.700	0.704	1	3
		Kα x (i)	6.682	1.7×10^{-5}	1	5
		Kα y (i)	6.668	0.069	1	3
		Kα z (f)	6.637	3.3×10^{-7}	1	3
Fe XXVI	6.966	Kα_1 (r)	6.973	0.277[c]	2	4
		Kα_2 (r)	6.952	0.139[c]	2	2

[a]With respect to H (Anders & Grevesse 1989). [b]Mean energy for the absorption lines considered in this paper, weighted on the oscillator strengths of the transitions contributing to the blend. [c]From Verner et al. (1996).

widths (EWs) of the absorption lines as a function of the ionization parameter and the column density of the intervening material, taking advantage of the code discussed by Nicastro, Fiore & Matt (1999). As for the emission lines, while we refer the reader to Bianchi & Matt (2002) for detailed calculations and plots, we devote Section 2.2 to a qualitative discussion on the relative contributions of resonance, intercombination and forbidden transitions to the total EWs for Fe XXV. Subsequently, we compare the theoretical results to an up-to-date list of observational evidence in favour of the presence of these features, to derive some physical parameters on the photoionized material responsible for their production.

2 THEORETICAL MODELS

Table 1 shows all the lines considered in this paper. The Fe XXV Kα complex includes four lines: three corresponding to the transition 1s^2–1s2p, subdivided into the resonance line w (^{1}S–^{1}P) and the two intercombination lines x (^{1}S–^{3}P$_2$) and y (^{1}S–^{3}P$_1$), and one to 1s^2–1s2s, that is the forbidden line z (^{1}S–^{3}S). On the other hand, the Fe XXVI Kα line is composed of a resonance doublet (1s–2p), similarly to neutral iron: the Kα_1 (^{2}S$_{1/2}$–^{2}P$_{3/2}$) and the Kα_2 (^{2}S$_{1/2}$–^{2}P$_{1/2}$). For Fe XXVI, the ratio 2:1 of the oscillator strengths for Kα_1 and Kα_2 is fixed because it depends only on the statistical weights of the two upper levels. On the other hand, the behaviour of the four He-like transitions is far more complex, depending on several physical parameters of the matter, and deserves a detailed, though qualitative, discussion. Satellite lines are *not* included in our calculations. Their possible relevance is discussed in Section 2.3.

2.1 Absorption lines

We consider the absorption features owing to resonance transitions from Fe XXV and Fe XXVI, including the intercombination y line for the former (see Table 1 for all the details). On the other hand, we do not consider in our calculations the He-like iron intercombination x and forbidden z lines, because their very low oscillator strengths make them negligible in absorption.

The EW of an absorption line can be expressed as

$$\mathrm{EW} = \int_0^{+\infty} [1 - \mathrm{e}^{-\tau_\nu}] \mathrm{d}\nu, \tag{1}$$

where τ_ν is the dimensionless frequency-specific optical depth of the considered transition:

$$\tau_\nu = \int_0^L \mathrm{d}s \alpha_\nu = n_l L \frac{\pi \mathrm{e}^2}{m_\mathrm{e} c} f_{lu} \Phi(\nu). \tag{2}$$

In this equation, n_l is the number density of the relevant ion in the lower level, while $\Phi(\nu)$ is the normalized Voigt profile, which basically depends on the natural width of the considered transition and the Doppler width of the line, which in turn is a function of the gas temperature and its turbulence, that is its dispersion velocity along the line of sight.

The relative abundances of the Fe XXV and Fe XXVI ions are calculated by means of the photoionization code CLOUDY (v. 94.00: Ferland 2000), as a function of the ionization parameter and the column density. Table 1 summarizes the input parameters chosen to model the continuum in our calculations, where not otherwise stated.

Following Bianchi & Matt (2002), we adopted a modified ionization parameter (similar to the one first proposed by Netzer 1996), which is more sensitive to the number of X-ray photons, so that our results are less dependent on the assumed continuum shape. The relation between this X-ray ionization parameter and the one adopted in CLOUDY is a function of the power-law index Γ (Bianchi & Matt 2002)

$$U_x = \frac{\int_2^{10} (L_E/E)\,\mathrm{d}E}{4\pi r^2 c n_\mathrm{e}} \implies \frac{U_x}{U}(\Gamma) = \frac{2^{1-\Gamma} - 10^{1-\Gamma}}{E_\mathrm{R}^{1-\Gamma}}, \tag{3}$$

where E_R is the energy equivalent in keV of 1 Ryd.

The integration of the Voigt profile in the different column density regimes was performed following the methods and the code developed by Nicastro et al. (1999), to which we refer the reader for details. All the calculations were performed separately for the four transitions considered in this paper, while only their final EWs were summed when stated. It should be noted that this paper also explores large column densities, where another useful diagnostic tool for this gas can be represented by the depth of the photoelectric edges, at $\simeq$8.8 (Fe XXV) and $\simeq$9.3 (Fe XXVI) keV. However, a full treatment of these edges is beyond the scopes of this work.

Figs 1 and 2 show the expected EWs for Fe XXV (resonant plus intercombination) and Fe XXVI (Kα_1 plus Kα_2) as a function of U_x and for different column densities. In these plots, the turbulence is assumed to be null. Fig. 3 shows the ratio between the EWs from the two ions, as a function of U_x. Indeed, the Fe XXV/Fe XXVI ratio, being not sensitive to the column density in the most interesting range of ionization (i.e. around $\log U_x = 0$ where the EWs of Fe XXV and Fe XXVI are equal as shown in Figs 1 and 2), can be used to measure the latter from the data.

The curve of growths for each transition separately are plotted in Fig. 4.[1] These curves, calculated at $\log U_x = 0$, give a feeling of the different contributions of the transitions to the total EW. Note that, for low column densities, their ratios are simply dictated by the

[1] See Nicastro et al. in preparation, Errata, for an explanation of the difference between the curve of growth for Fe XXVI plotted here and that plotted in fig. 1 of the original work by Nicastro et al. (1999).

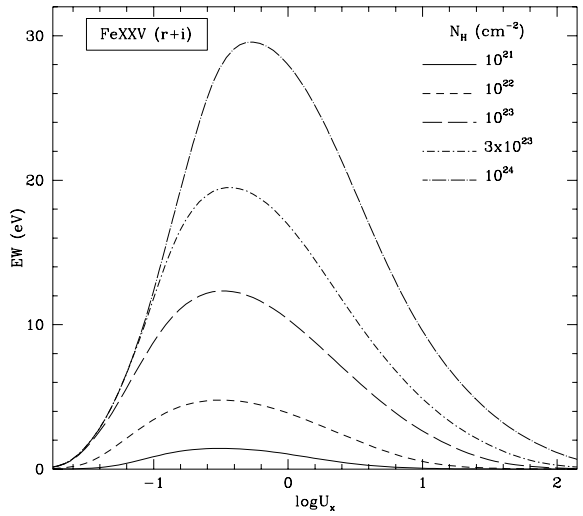

Figure 1. EW for the Fe XXV Kα absorption complex (resonant + intercombination) as a function of U_x, for different values of column densities. See Table 1 for the parameters adopted in the calculations. The turbulent velocity is set equal to zero.

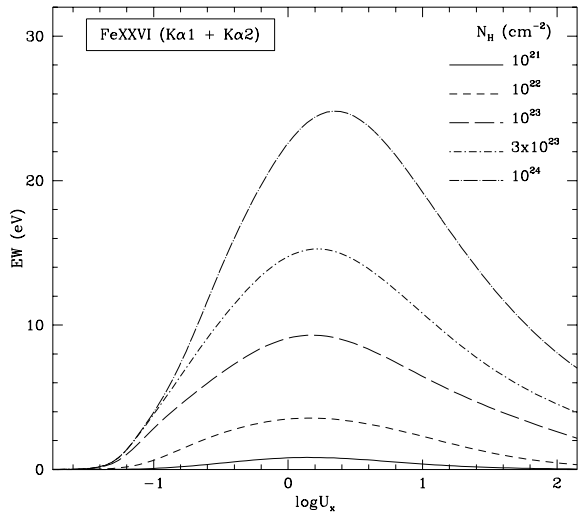

Figure 2. EW for the Fe XXVI Kα absorption complex (Kα_1 + Kα_2) as a function of U_x, for different values of column densities. See Table 1 for the parameters adopted in the calculations. The turbulent velocity is set equal to zero.

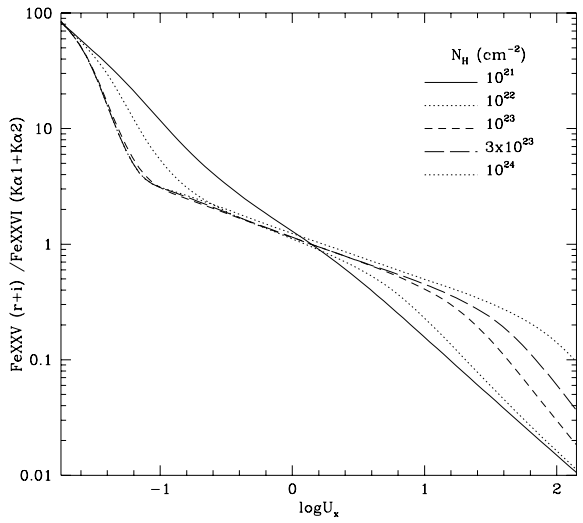

Figure 3. Ratio of the absorption lines EWs of the Fe XXV Kα absorption complex (resonant + intercombination) over Fe XXVI (Kα_1 + Kα_2) as a function of U_x, for different values of column densities. See Table 1 for the parameters adopted in the calculations. The turbulent velocity is set equal to zero.

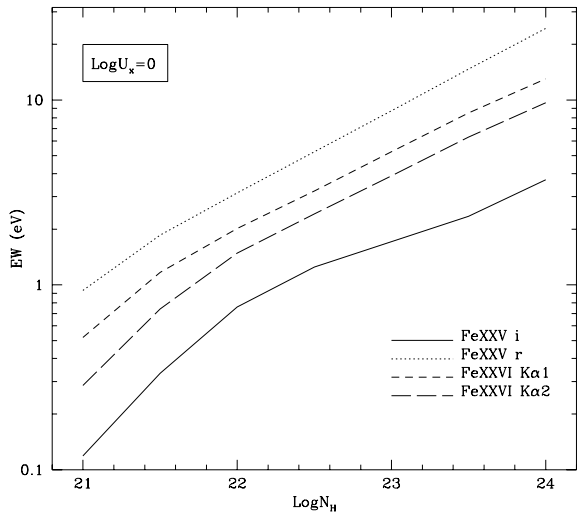

Figure 4. Curve of growth for the four transitions considered in this paper, with $\log U_x = 0$. See Table 1 for the parameters adopted in the calculations. The turbulent velocity is set equal to zero.

ratios of their oscillator strengths, while some deviations, though quite marginal, can be observed at larger column densities.

We now consider the effects of the turbulence. At a temperature of $T = 10^6$ K, the mean thermal velocity of iron ions is generally expressed by the Doppler parameter

$$b \equiv \sqrt{\frac{2kT}{M}} \simeq 17\,\mathrm{km\,s^{-1}}, \tag{4}$$

which means that, for any velocity dispersion larger than $\sigma_v \simeq 100\,\mathrm{km\,s^{-1}}$, the thermal motion will contribute less than 15 per cent to the total Doppler broadening. Note that turbulent velocities of that order are easily reached in a gas in Keplerian motion at a parsec scale around a SuperMassive BH, so that they should be included in a realistic model.

Indeed, the effect of turbulence can be very important, because it broadens the line profile, effectively raising the column of gas needed for the line core to become optically thick. Nicastro et al. (1999) have calculated that the optical depth to resonant absorption of a column of gas under strong turbulence (i.e. σ_v larger than $300\,\mathrm{km\,s^{-1}}$) can be more than 10 times lower than the same column of gas unaffected by turbulence. As a result, the curve of growth of the line saturates at a larger column density, allowing the EW to rise linearly over a wider range of N_H. This is shown in Figs 5 and 6: the resulting EWs can reach 100 eV for $N_H \simeq 10^{24}\,\mathrm{cm^{-2}}$.

Finally, we explored the effects owing to a different set of input parameters for the incident continuum, in terms of temperature, photon index and density. As found by Bianchi & Matt (2002) for the emission lines, the results are basically the same for a wide range

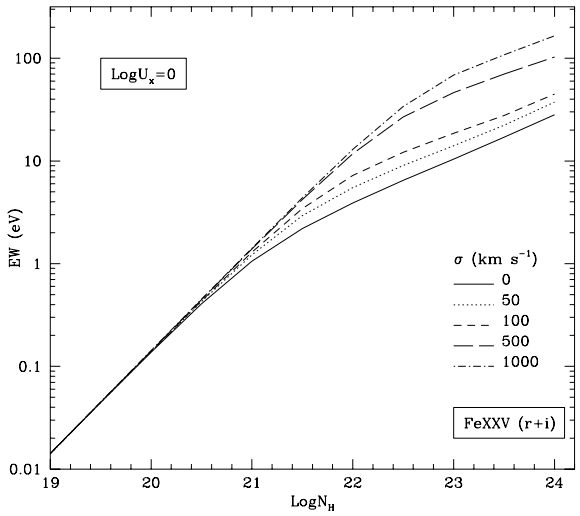

Figure 5. Curve of growth for the Fe XXV Kα absorption complex (resonant + intercombination) for different values of turbulence.

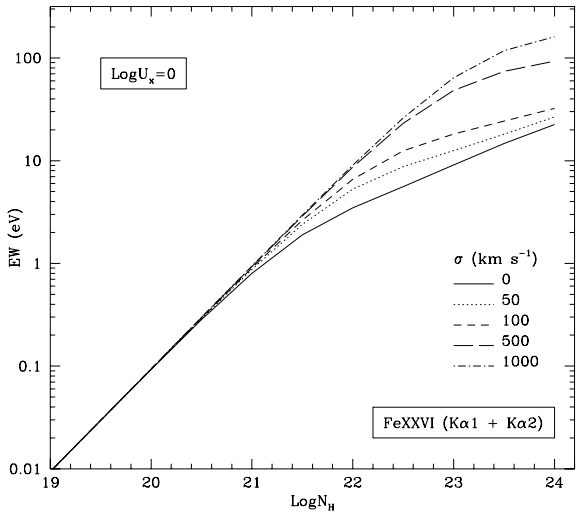

Figure 6. Curve of growth for the Fe XXVI Kα absorption complex (Kα_1 + Kα_2) for different values of turbulence.

of gas densities, because it turns out to be equivalent to changing the distance between the source and the gas, while leaving the same ionization parameter. On the other hand, an almost negligible variation in the position and/or the value of the maximum is found for plots 1 and 2 when different values of Γ are explored, thanks to our choice of the X-ray ionization parameter. A quantitatively more significant dependence on temperature is instead found, owing to the larger contribution of collisional ionization as T increases, thus shifting to lower values the ionization parameter corresponding to large abundances of Fe XXV and Fe XXVI. However, all these effects are similar to those presented by Bianchi & Matt (2002) and therefore are not further discussed here.

2.2 Emission lines

Emission lines from Fe XXV and Fe XXVI in unobscured AGN were treated in detail by Bianchi & Matt (2002), to whom we refer the reader for details on calculations and for plots similar to the ones presented in this paper for the absorption features.

Fe XXV emission lines are produced by recombination and resonant scattering (see Matt, Brandt & Fabian 1996; Bianchi & Matt 2002, and references therein). Recombination lines in a photoionized matter are generally described by introducing an effective fluorescent yield which represents the probability that the recombination cascade includes the radiative emission of a Kα photon. This process can be treated analytically in the Compton-thin regime, which is appropriate for column densities up to $\simeq 10^{24}$ cm^{-2}. As pointed out by several authors (see e.g. Porquet & Dubau 2000; Bautista & Kallman 2000), photoionized gas is characterized by weak emission from the resonant w line, while for iron the two intercombination lines x+y contribute almost equally with the forbidden z line to the total emission feature, for a wide range of densities. Therefore, if the lines are not resolved by the X-ray instruments, a single feature with centroid around 6.66 keV should come out from recombination processes in a photoionized gas.

Resonantly scattered Kα lines are instead the result of radiative de-excitation after excitation owing to the absorption of continuum photons at the energy of the line. As illustrated in Section 2.1, the dominant absorption transition is the resonant w, followed by the intercombination y. As the latter has an oscillator strength which is 10 per cent of the former, we expect that this ratio is preserved in the emission process. The contribution from x and z is completely negligible. Again, if the resolution of the X-ray detector is lower than the separation between the w and the y line, we should observe a blended feature around 6.70 keV. This process is much more effective than recombination so that lines produced in this way are dominant in the optically thin regime. However, its cross-section is much larger than in the previous case, so that the gas becomes rapidly optically thick to resonant scattering. By means of Monte Carlo simulations, Matt et al. (1996) showed that a column density as small as 5×10^{20} cm^{-2} is enough to significantly reduce the EWs from these lines. As a consequence, when $N_{\rm H}$ becomes greater than $\simeq 10^{23}$ cm^{-2}, recombination becomes the dominant process.

Fig. 7 summarizes these considerations, showing a plot of the relative contributions of each transition as a function of the column density of the gas. The plot takes into account the effect owing to the saturation of the resonant line when the column density increases

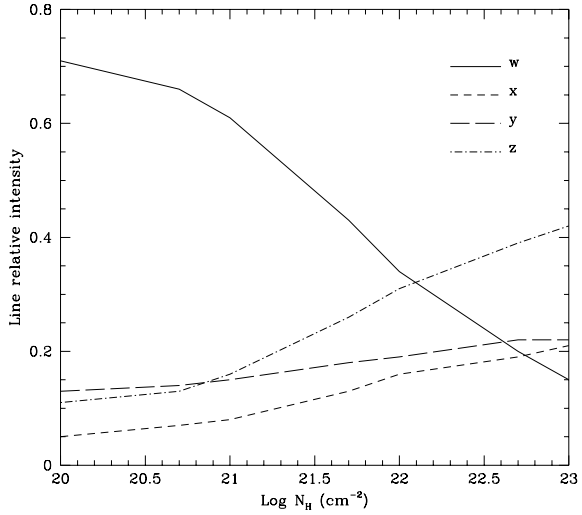

Figure 7. Relative intensity of Fe XXV w, x, y and z transitions versus the column density of the gas. The turbulent velocity is set equal to zero. Note that this is a rough plot: see text for details and caveats.

(from fig. 5 of Matt et al. 1996) and the discussion above about the ratios between w, x, y and z when produced by recombination or resonant scattering. As a result, the resonant w line dominates the emission spectrum up to $10^{22}\,\mathrm{cm}^{-2}$ and then is reached and overcome by the forbidden line z and the two intercombination x and y. These results are in good agreement with the recent calculations performed by Coupé et al. (2004).

Note that the total EW for the Fe XXV is the one calculated by Bianchi & Matt (2002), while Fig. 7 simply contains the information on how this EW should be divided among the different lines. Therefore, an high-resolution spectrum of the He-like iron Kα emission line complex produced in photoionized gas has, at least in principle, the potentiality to reveal the column density of the gas where the lines are produced, similarly to what Kinkhabwala et al. (2002) already showed for lighter metals in the soft X-ray spectrum of NGC 1068. Moreover, it can also be useful to note that, even if the resolution of the observed spectrum does not allow one to resolve the single lines, it could still be possible to appreciate the difference between a 6.70-keV line at low column densities and a 6.66-keV line at larger N_{H} values.

Another interesting consequence of these results is the possibility of observing simultaneously absorption and emission features from the same ionic species. As an example, let us consider a large covering factor gas, with high column density and lying *also* along the line of sight. In this case the resonant line w would not be produced in emission, but only absorbed, while x, y and z lines would dominate the emission He-like iron complex. Therefore, the observed spectrum would show the intercombination and forbidden lines in emission (the y line partly diluted by absorption), while the resonant line would be apparent only in absorption: such an observation is in principle within reach of *Astro-E2*.

However, we would like to point out some cautionary warnings on these results. Fig. 7 does not intend to be a detailed description of such a complex issue, but simply displays a rough behaviour deriving from the above-mentioned effects. The plot was produced in the transmission case, when the observer looks at the photons which come out from the cloud: in the reflection case, the dominance of resonant scattering at low column densities is enhanced, but the differences are not very significant for the observed spectrum (see Matt et al. 1996; Bianchi & Matt 2002, for details). It should also be reminded that inner-shell ionization of Fe XXIV is an additional mechanism in populating the upper level of the forbidden line (metastable level), hence if the ionic abundance of Fe XXIV is significant, this process can enhance the values of z plotted in Fig. 7. This can be the case in transient plasma as shown by Mewe & Schrijver (1975). Another contribution not considered in the plot is that from turbulence. As explained for the absorption lines in Section 2.1, turbulence broadens the line profile, so that the gas becomes optically thick to resonant scattering at a larger column density. As a consequence, the value of N_{H} which separates the regimes where recombination or resonant scattering dominates increases with the amount of turbulence. As a final remark, note that we assumed that the gas was in pure photoionization equilibrium: any deviation from this ideal situation could change significantly the ratio between the He-like emission lines.

2.3 Satellite lines

Satellite lines are systems of lines appearing close to or blended with the main lines of highly charged ionized atoms. These lines can either correspond to the stabilizing transitions in the process of dielectronic recombination (dielectronic satellite lines) or by inner-shell electron/photon excitation (inner-shell excitation satellite lines). As shown by Oelgoetz & Pradhan (2001) dielectronic satellite lines in hot plasmas (i.e. collisional plasmas) dominate the Kα emission at temperatures well below the one corresponding to the maximum of ionic abundance of FeXXV, i.e. $T < T_{\mathrm{m}}$ which is approximatively $10^{7.4}$ K (Arnaud & Rothenflug 1985).

Table 2. Experimental energies of the Fe XXV lines and of the satellite lines of Fe XXIV and Fe XXIII (data from Decaux et al. 1997).

Ion	Transition	Label	E (keV)	f_{ij}
Fe XXV	$1s^2\ {}^1S_0$–$1s\,2p\ {}^1P_1$	w	6.700	0.704[a]
Fe XXV	$1s^2\ {}^1S_0$–$1s\,2p\ {}^3P_2$	x	6.683	
Fe XXIV	$1s^2\,2s\ {}^2S_{1/2}$–$1s\,2s\,2p\ ({}^1P)\ {}^2P_{1/2}$	t	6.676	0.110[b]
Fe XXV	$1s^2\ {}^1S_0$–$1s\,2p\ {}^3P_1$	y	6.668	0.069[a]
Fe XXIV	$1s^2\,2s\ {}^2S_{1/2}$–$1s\,2s\,2p\ ({}^3P)\ {}^2P_{3/2}$	q	6.662	0.469[c]
Fe XXIV	$1s^2\,2s\ {}^2S_{1/2}$–$1s\,2s\,2p\ ({}^3P)\ {}^2P_{1/2}$	r	6.653	0.147[c]
Fe XXV	$1s^2\ {}^1S_0$–$1s\,2p\ {}^3S_1$	z	6.637	
Fe XXIII	$1s^2\,2s^2\ {}^1S_0$–$1s\,2s^2\,2p\ {}^1P_1$	β	6.629	0.666[c]

The oscillator strengths (f_{ij}) greater than 0.05 are given from: [a]NIST (see Table 1); [b]Nahar, Pradhan & Zhang (2001); and [c]Behar & Netzer (2002).

On the contrary, the satellite lines to the Fe XXV lines (w, x, y, z) owing to inner-shell photoexcitation of Li-like iron (Fe XXIV) or Be-like iron (Fe XXIII) can be significant, i.e.

$1s^2\,2s + \mathrm{photon} \rightarrow 1s\,2s\,2p$ (satellite lines: q, r, s, t)

$1s^2\,2s^2 + \mathrm{photon} \rightarrow 1s\,2s^2\,2p$ (satellite line: β).

Table 2 reports the experimental energies of the satellite lines in the vicinity of the w, x, y and z lines (Decaux et al. 1997). The values reported in Table 1 from the National Institute of Standards and Technology (NIST) data base are in excellent agreement with these experimental energies. The oscillator strengths greater than 0.05 are given to show which lines are expected to be significant in both absorption and emission. The two strongest satellite lines would be q (Li-like) and β (Be-like) depending on the relative abundance of Fe XXIV and Fe XXIII, respectively.

The spectral resolution of the XRS (X-Ray Spectrometer) on board *Astro-E2* will be of the order of 6 eV at 6.6–6.7 keV (Fe XXV lines). The lines x and t ($\Delta E_{x-t} = 7$ eV), and the lines z and β ($\Delta E_{z-\beta} = 8$ eV) can thus be resolved. The lines y and q are separated by 6 eV which is close to the resolving power of the XRS, and it will be possible to infer the intensity of the line by line profile deconvolution. We remind that the resolving power of *Astro-E2* XRS is much larger than the thermal line width for iron at 10^6 keV

Table 3. Fe XXV and Fe XXVI emission lines in three of the brightest Compton-thick Seyfert galaxies. A reference to this paper (TP) means that data were re-analysed to add some values not found in the literature (in these cases, numbers are indicated in italics).

Source	Instr. (Date)	Fe XXV		Fe XXVI		Ref.
	(mm/yy)	EW[a] (eV)	I^b	EW[a] (eV)	I^b	
NGC 1068	EPIC pn (07/00)	w (6.725 ± 0.001 keV): 1430^{+195}_{-130}	$2.2^{+0.3}_{-0.2}$	494^{+210}_{-70}	$0.7^{+0.3}_{-0.1}$	Matt et al. (2004b)
		z ($6.61^{+0.01}_{-0.04}$ keV): 485^{+120}_{-60}	$0.8^{+0.2}_{-0.1}$			
	ACIS HETG (02/00)	w (6.73 ± 0.02 keV): *1000 ± 500*	1.5 ± 0.7	*<800*	<1.1	Ogle et al. (2003), TP
		z (6.59 ± 0.02 keV): *1000 ± 500*	1.6 ± 0.7			
Circinus	EPIC pn (08/01)	*420 ± 60*	1.4 ± 0.2	*250^{+160}_{-130}*	*$0.8^{+0.5}_{-0.4}$*	Molendi et al. (2003), TP
	ACIS HETG (06/00)	*800 ± 330*	2.7 ± 1.1	*<310*	*<2.6*	Sambruna et al. (2001)
Mrk 3	EPIC pn (10/00)	4800 ± 2400	0.4 ± 0.2	<1500	<0.1	Bianchi et al. in preparation
	ACIS HETG (03/00)	*$11\,000^{+9000}_{-4000}$*	*$0.9^{+0.7}_{-0.3}$*	*<10 000*	*<2.0*	Sako et al. (2000), TP

[a]Calculated against the reflected continuum only. [b]10^{-5} photon cm^{-2} s^{-1}.

(well below 1 eV), while it corresponds to a turbulence velocity of about 270 km s^{-1}. Therefore, in the case of significant line broadening owing to turbulence, the contribution of the satellite lines to the four lines of Fe XXV has to be taken into account.

Finally, in very dense plasmas the $1s^2\,2p$ level can be populated and one can, for example, obtain: $1s^2\,2p$ + photon $\rightarrow$ $1s\,2p^2$ [satellite lines: k (6.654 keV), j (6.644 keV)]. However, in this work we consider a plasma with a electron density of 10^6 cm^{-3} (Table 1), and therefore the satellite lines k, and j can be neglected here. For Fe XXVI, no inner-shell excitation satellite line of Fe XXV exists.

In conclusion, in the case of negligible turbulence velocity, i.e. less than about 270 km s^{-1}, the satellite lines are unblended or are easily separated by line profile deconvolution to the four lines of Fe XXV and the lines intensities reported in this paper can be used safely for spectral analysis of *Astro-E2*–XRS observations.

3 OBSERVATIONAL EVIDENCE

Tables 3 and 4 show a complete (as far as we know) list of objects (Compton thick and unobscured/Compton thin, respectively) where emission and/or absorption lines from Fe XXV and Fe XXVI were detected by either *Chandra* or *XMM–Newton*. The listed values are those reported in the literature, as found in the cited references. When some of the needed values were not present in these works, we re-analysed the relative spectra and extracted the required information. Finally, for some objects we found in the archives *XMM–Newton* and/or *Chandra* unpublished data: we analysed them for the first time and included them in the table. Standard procedures for data reduction were adopted (see e.g. Bianchi et al. 2004).

3.1 Compton-thick objects

Compton-thick Seyfert galaxies, i.e. objects obscured by a column density larger than $\sigma_{\rm T}^{-1} = 1.5 \times 10^{24}$ cm^{-2}, are the best-suited objects for the observation of ionized iron lines in emission, as the primary continuum is completely suppressed in this band and hence these lines are not diluted by this component. We present in Table 3 *Chandra* and *XMM–Newton* results from three of the brightest Compton-thick Seyfert galaxies, that is NGC 1068, Circinus and Mrk 3.

The most interesting object is NGC 1068, where the resonant w and the forbidden z lines are actually resolved in the *XMM–Newton* data. The ratio of their fluxes, $F_w/F_z = 2.8 \pm 0.8$, points towards a gas column density range roughly of $\log N_{\rm H} = 21$–21.5 (see Fig. 7). On the other hand, an ionization parameter around $\log U_x = -0.5$ can be measured from the ratio between the Fe XXV and Fe XXVI EWs, thus requiring an iron overabundance of a factor $\simeq$2 with respect to the solar values to obtain the total EW of each line (see figs 2–5 from Bianchi & Matt 2002). Note that such an overabundance was also measured from the depth of the iron edge in the European Photon Imaging Camera (EPIC) pn data (Matt et al. 2004b): even if these values correspond to two different materials, it is suggestive that they are similar.

A much lower flux ratio between the the resonant w and the forbidden z lines is instead measured in the *Chandra* data. Even if this value is still consistent within the errors of those found in the *XMM–Newton* data and the two lines are not resolved in the HETG spectrum, being actually the result of a de-blending of a single feature (see Ogle et al. 2003), it may still give some indications on the geometry of the photoionized reflector. In particular, Ogle et al. (2003) noted that this region should be extended on a 3-arcsec scale, implying that the HETG spectrum includes only the inner region, while the EPIC pn clearly observes all the gas. In this case, it is possible that the gas which is closer to the nucleus has a larger column density, enhancing the production of the forbidden line, while the outer regions, which dominate the pn spectrum, have a lower column density. However, the nuclear region in NGC 1068 accounts for the major part of the flux (Young, Wilson & Shopbell 2001; Brinkman et al. 2002; Ogle et al. 2003), so that any contribution from the extended region to the total EPIC pn spectrum should be small. Moreover, this scenario is at odds with the fact that the total fluxes of the Fe XXV features seem constant between the two data sets, but the very large errors on the *Chandra* flux values prevent us from drawing any firm conclusions.

As a final remark on NGC 1068, we note that the centroid energies for the Fe XXV lines are formally inconsistent with their expected values, both in the EPIC pn and in the *Chandra* spectra. This is puzzling, because in both observations a blueshift for the w line and a redshift for the z line are implied, at odds with a common origin in the same material. Moreover, the Fe XXVI line energy ($6.92^{+0.01}_{-0.04}$ keV: Matt et al. 2004b) also implies a redshift. While a less than perfect calibration can be invoked for both instruments, we do not have any other satisfactory explanation for this result.

The other two Compton-thick sources have ionized iron lines much weaker with respect to the total continuum and to the neutral iron line, so that the statistics do not allow us to resolve the single transitions. However, in the case of Mrk 3, a best-fitting value of $6.71^{+0.03}_{-0.02}$ keV for the Fe XXV line (Bianchi et al. 2005) seems to indicate that the resonant line is also the dominant one in this source,

Table 4. A list of objects where emission and/or absorption lines from Fe XXV and Fe XXVI were detected (see text for details). A reference to this paper (TP) means that data were re-analysed to add some values not found in literature (in these cases, numbers are indicated in italics) or that the relative observation was analysed for the first time.

Source	Instr. (Date) (mm/yy)	Fe XXV EW (eV)	Fe XXV I^a	Fe XXVI EW (eV)	Fe XXVI I^a	Ref.
		Emission lines				
NGC 5506	ACIS HETG (12/00)	*< 31*	*< 2.4*	*< 26*	*< 1.7*	Bianchi et al. (2003a), TP
	EPIC pn (02/01)	27^{+17}_{-12}	$2.0^{+1.3}_{-0.9}$	41^{+11}_{-27}	$2.0^{+0.5}_{-1.3}$	
	EPIC pn (01/02)	$\mathit{19}^{+\mathit{11}}_{-\mathit{12}}$	$\mathit{2.3}^{+\mathit{1.5}}_{-\mathit{1.4}}$	*19 ± 13*	$\mathit{2.0}^{+\mathit{1.5}}_{-\mathit{1.4}}$	
NGC 7213	EPIC pn (05/01)	25^{+10}_{-13}	0.6 ± 0.3	22 ± 14	0.5 ± 0.3	Bianchi et al. (2003b)
NGC 7314	EPIC pn (05/01)	*16 ± 11*	*0.7 ± 0.5*	*28 ± 13*	*1.1 ± 0.5*	TP
	ACIS HETG (07/02)	29^{+20}_{-17}	$1.1^{+0.7}_{-0.6}$	63^{+33}_{-23}	$1.9^{+1.0}_{-0.7}$	Yaqoob et al. (2003)
IC 4329A	EPIC pn (01/01)	*< 13*	*< 2.1*	*< 48*	*< 6.3*	TP
	ACIS HETG (08/01)	<17	*< 4.6*	42^{+30}_{-21}	$6.2^{+4.4}_{-3.1}$	McKernan & Yaqoob (2004), TP
NGC4593	ACIS HETG (06/01)	*< 31*	*< 1.5*	*< 72*	*< 2.7*	TP
	EPIC pn (06/02)	<13	*< 1.0*	39 ± 13	$\mathit{1.4}^{+\mathit{1.1}}_{-\mathit{0.6}}$	Reynolds et al. (2004), TP
MCG-2-58-22	EPIC pn (12/00)	*< 44*	*< 1.6*	$\mathit{55}^{+\mathit{26}}_{-\mathit{35}}$	$\mathit{1.8}^{+\mathit{0.8}}_{-\mathit{1.1}}$	TP
MRK 205	EPIC pn (05/00)	35 ± 17	*0.2 ± 0.1*	51 ± 19	*0.3 ± 0.1*	Reeves et al. (2001), TP
NGC 3783	EPIC pn (12/01)	–[b]	–[b]	17 ± 5	1.4 ± 0.3	Reeves et al. (2004)
ESO198-G024	EPIC pn (12/00)	*< 80*	*< 0.9*	*< 65*	*< 1.0*	TP
	EPIC pn (01/01)	*< 28*	*< 0.4*	*< 63*	*< 0.8*	
	ACIS-S (04/04)	*< 15*	*< 0.1*	$\mathit{56}^{+\mathit{49}}_{-\mathit{35}}$	*0.3 ± 0.2*	
		Absorption lines				
NGC 4507	EPIC pn (01/01)	*> −16*	–[c]	*> −24*	–[c]	Matt et al. (2004a), TP
	ACIS HETG (03/01)	−26 ± 16	–[c]	*> −12*	–[c]	
MCG-6-30-15	EPIC pn (07/00+07/01)	−11 ± 6	–[c]	–[d]	–[c]	Vaughan & Fabian (2004)
NGC 3783	EPIC pn (12/01)	−17 ± 5	–[c]	–[b]	–[c]	Reeves et al. (2004)
	ACIS HETG (01/00+06/01)	−13 ± 5	–[c]	–[b]	–[c]	Kaspi et al. (2002)

[a] 10^{-5} photon cm^{-2} s^{-1}. [b] Fluxes are not considered for variability in absorption lines (see text for details). [c] Values are not calculated because a line in emission (absorption) of the same ionic species is present in the spectrum. [d] A detailed analysis of this complex spectrum, which includes EPIC pn and MOS data from two observations, is beyond the scope of this paper.

again suggesting a low column density. In both sources, the He-like line is much stronger than the H-like one, so that the ionization parameter should not exceed $\log U_X \simeq -0.5$. From the observed EWs, an iron overabundance of at least a factor of 2 is needed for Mrk 3, while a value closer to 1 is required for Circinus, as again found from the depth of the iron edge (Molendi, Bianchi & Matt 2003).

Finally, it must be mentioned that there are two other Compton-thick sources bright enough to allow a detailed spectral analysis, i.e. NGC 6240 and 4945 (Matt et al. 2000). In the former source both the He- and the H-like iron lines are detected (Boller et al. 2003), while in the latter only the He-like one is visible (Schurch, Roberts & Warwick 2002). However, as argued in the abovementioned papers, it is possible that in these two sources, which have strong starburst regions, the lines are emitted in collisionally ionized plasma, and therefore we do not discuss them here.

3.2 Unobscured and Compton-thin objects

The sample in Table 4 includes most type 1 Seyfert galaxies, some intermediate objects and a Compton-thin type 2 Seyfert galaxy (NGC 4507). As for the X-ray properties, all the sources are either unobscured or the absorbing column density from neutral matter allows direct observation of the nuclear continuum at the iron line *K* band.

All three sources with absorption lines present only a feature from He-like iron, thus implying $\log U_x < 0$ (Fig. 3). The observed EWs can be produced by column densities around 10^{23} cm^{-2}, except for NGC 4507 which needs a larger $N_{\rm H}$, unless effects from turbulence and/or iron abundance are taken into account.

On the other hand, it is interesting to note that four out of the nine sources where emission lines are observed have indeed features both from Fe XXV and Fe XXVI. In these cases, an ionization parameter around $\log U_x = 0$–0.5 is required. The observed EWs are so large to imply column densities larger than 10^{23} cm^{-2} and/or iron overabundance by a factor of 2–3. This is also true for the remaining objects, where only the H-like line is observed, even if an higher ionization parameter (around $\log U_x = 0.5$) is appropriate in these cases. However, it is important to stress that the errors on the EWs are generally so large to possibly reduce the need for iron overabundance in many cases.

NGC 3783 is the only object whose spectrum displays both an absorption and an emission line. These lines are from different ionic

species, respectively from Fe XXV and Fe XXVI. As one is seen in absorption and the other in emission, they must be produced at least in two different clouds, the former being along the line of sight. If this is the case, the two clouds may well have different values of the ionization parameter, because of a different value of the density or of the distance from the source. Under these conditions, column densities of few 10^{22} cm^{-2} and $\log U_x \simeq -0.5$–0 can be responsible for the observed EW of the cloud seen in emission, while $N_{\rm H}$ values larger by an order of magnitude and $\log U_x \simeq 0$–0.5 are required for the one in absorption. No particular need for overabundance or other corrections are required.

Unfortunately, the quality of present spectra does not allow us to take advantage of the He-like diagnostics presented in the previous section, because the energy resolution is not good enough to disentangle the contributions from the single transitions. On the other hand, the effective area of the instruments does not provide enough statistics to measure the centroid energy of these weak lines with a precision sufficient to check for a clear difference between a recombination or resonant scattering dominated regime.

The larger occurrence of emission lines with respect to absorption lines in Table 4 may give us some information on the covering factor $f_{\rm c}$ of the photoionized material, i.e. the solid angle subtended by the gas under investigation. Indeed, a prevalence of emission lines with large EWs is expected for large $f_{\rm c}$ values, even if this relation is not linear for high column densities and when additional effects are taken into account, so that the maximum emission is typically for $f_{\rm c} \simeq 0.5 - 0.7$ (Netzer 1993, 1996). On the other hand, absorption lines are dominant when a small covering factor cloud ($f_{\rm c} < 0.1$) lies exactly along the line of sight, so that the emission lines from other directions gives a negligible contribution to the overall spectrum, as in the case adopted by Nicastro et al. (1999). Therefore, even if it is likely that in low-quality spectra emission lines are easier to observe than absorption features, we can conclude that the gas we are studying generally subtends a considerable solid angle with respect to the illuminating source.

The flux variability of the observed emission lines could, in principle, be another tool to investigate the geometrical properties of the gas that produces them. Indeed, a variation of the line flux would imply a response of the reflected spectrum to a variation of the illuminating source, with a delay proportional to the distance of the reflecting medium. In all the cases where we have more than one observation, no variation in the fluxes of the lines are detected. Even if this result is not very strong owing to the large errors in the data, it is still an indication that the region responsible for the production of the lines from Fe XXV and Fe XXVI should be located at a distance at least of the order of light-months (up to years in many cases) from the illuminating source.

As for the absorption lines, the relevant parameter for variability is not the flux, but the EW. In NGC 3783, Reeves et al. (2004) reported a significant EW variability within the same observation, implying a change in the properties of the gas over a time-scale smaller than 10^5 s. However, the integrated EW of the six *Chandra* observations analysed by Kaspi et al. (2002) is still consistent with that measured in the total EPIC pn spectrum and no variability was found in the soft X-ray spectrum of this source (Behar et al. 2003; Netzer et al. 2003). On the other hand, Vaughan & Fabian (2004) reported an EW variability in the absorption line of MCG-6-30-15 between the two EPIC observations taken a year apart. The interpretation of such variations is less straightforward than for the emission lines, because it may be in principle owing to either a change in the ionization structure of the gas or in its column density along the line of sight.

4 CONCLUSIONS

We have calculated the EWs of the absorption lines produced by Fe XXV and Fe XXVI in a Compton-thin, low-velocity photoionized material illuminated by the nuclear continuum in AGN. We found that our results are consistent with the observations, provided there are column densities of the gas of around 10^{23} cm^{-2} or larger. However, we have shown that these values can be effectively reduced if the effects owing to turbulence are taken in account.

On the other hand, the comparison of similar calculations for the emission lines (as presented by Bianchi & Matt 2002) with an up-to-date list of known unobscured (at least at the iron line) Seyfert galaxies generally results in the need for an iron overabundance by a factor of 2–3. However, it should be stressed that the error bars on the observed EWs are still too large to reach a firm conclusion. The much larger occurrence of emission lines with respect to the absorption ones in the analysed spectra gives an hint that the covering factor of the photoionized gas under investigation is likely quite large.

Finally, we have shown that the relative contributions of the single transitions of Fe XXV w, x, y and z in the regimes where recombination or resonant scattering dominates provides a useful diagnostic tool to measure the column density of the gas. This effect must be taken into account with future, high-resolution missions, like *Astro-E2*. In the meantime, we have shown that in the high-quality EPIC pn spectrum of the Compton-thick Seyfert galaxy NGC 1068, the forbidden z and the resonant w lines are actually resolved and their flux ratio implies a column density range of $\log N_{\rm H} = 21$–21.5, in excellent agreement with the value expected from the total EW.

ACKNOWLEDGMENTS

SB and GM acknowledge ASI and MIUR (under Grant No. COFIN-03-02-23) for financial support.

REFERENCES

Anders E., Grevesse N., 1989, Geochim. Cosmochim. Acta, 53, 197
Antonucci R., 1993, ARA&A, 31, 473
Arnaud M., Rothenflug R., 1985, A&AS, 60, 425
Bautista M. A., Kallman T. R., 2000, ApJ, 544, 581
Behar E., Netzer H., 2002, ApJ, 570, 165
Behar E., Rasmussen A. P., Blustin A. J., Sako M., Kahn S. M., Kaastra J. S., Branduardi-Raymont G., Steenbrugge K. C., 2003, ApJ, 598, 232
Bely-Dubau F., Faucher P., Dubau J., Gabriel A. H., 1982, MNRAS, 198, 239
Bianchi S., Matt G., 2002, A&A, 387, 76
Bianchi S., Balestra I., Matt G., Guainazzi M., Perola G. C., 2003a, A&A, 402, 141
Bianchi S., Matt G., Balestra I., Perola G. C., 2003b, A&A, 407, L21
Bianchi S., Matt G., Balestra I., Guainazzi M., Perola G. C., 2004, A&A, 422, 65
Bianchi S., Miniutti G., Fabian A. C., Iwasawa K., 2005, MNRAS, submitted
Boller T., Keil R., Hasinger G., Costantini E., Fujimoto R., Anabuki N., Lehmann I., Gallo L., 2003, A&A, 411, 63
Brinkman A. C., Kaastra J. S., van der Meer R. L. J., Kinkhabwala A., Behar E., Kahn S. M., Paerels F. B. S., Sako M., 2002, A&A, 396, 761
Coupé S., Godet O., Dumont A.-M., Collin S., 2004, A&A, 414, 979
Decaux V., Beiersdorfer P., Kahn S. M., Jacobs V. L., 1997, ApJ, 482, 1076
Ferland G. J., 2000, in Arthur J., Brickhouse N., Franco J., eds, Rev. Mex. Astron. Astrofis. Ser. Conf. Astrophysical Plasmas Codes, Models, and Observations. UNAM, Mexico, p. 153
Kaspi S. et al., 2002, ApJ, 574, 643
Kinkhabwala A. et al., 2002, ApJ, 575, 732
McKernan B., Yaqoob T., 2004, ApJ, 608, 157
Matt G., Brandt W. N., Fabian A. C., 1996, MNRAS, 280, 823

Matt G., Fabian A. C., Guainazzi M., Iwasawa K., Bassani L., Malaguti G., 2000, MNRAS, 318, 173
Matt G., Bianchi S., D 'Ammando F., Martocchia A., 2004a, A&A, 421, 473
Matt G., Bianchi S., Guainazzi M., Molendi S., 2004b, A&A, 414, 155
Mewe R., Schrijver J., 1975, Ap&SS, 38, 345
Molendi S., Bianchi S., Matt G., 2003, MNRAS, 343, L1
Nahar S. N., Pradhan A. K., Zhang H. L., 2001, Phys. Rev. A, 63, 060701
Netzer H., 1993, ApJ, 411, 594
Netzer H., 1996, ApJ, 473, 781
Netzer H. et al., 2003, ApJ, 599, 933
Nicastro F., Fiore F., Matt G., 1999, ApJ, 517, 108
Oelgoetz J., Pradhan A. K., 2001, MNRAS, 327, L42
Ogle P. M., Brookings T., Canizares C. R., Lee J. C., Marshall H. L., 2003, A&A, 402, 849
Porquet D., Dubau J., 2000, A&AS, 143, 495
Pounds K. A., Reeves J. N., Page K. L., Wynn G. A., O 'Brien P. T., 2003, MNRAS, 342, 1147
Reeves J. N., Turner M. J. L., Pounds K. A., O 'Brien P. T., Boller T., Ferrando P., Kendziorra E., Vercellone S., 2001, A&A, 365, L134
Reeves J. N., O 'Brien P. T., Ward M. J., 2003, ApJ, 593, L65
Reeves J. N., Nandra K., George I. M., Pounds K. A., Turner T. J., Yaqoob T., 2004, ApJ, 602, 648
Reynolds C. S., Brenneman L. W., Wilms J., Kaiser M. E., 2004, MNRAS, 352, 205
Sako M., Kahn S. M., Paerels F., Liedahl D. A., 2000, ApJ, 543, L115
Sambruna R. M., Netzer H., Kaspi S., Brandt W. N., Chartas G., Garmire G. P., Nousek J. A., Weaver K. A., 2001, ApJ, 546, L13
Schurch N. J., Roberts T. P., Warwick R. S., 2002, MNRAS, 335, 241
Vaughan S., Fabian A. C., 2004, MNRAS, 348, 1415
Verner D. A., Verner E. M., Ferland G. J., 1996, At. Data Nucl. Data Tables, 64, 1
Yaqoob T., George I. M., Kallman T. R., Padmanabhan U., Weaver K. A., Turner T. J., 2003, ApJ, 596, 85
Young A. J., Wilson A. S., Shopbell P. L., 2001, ApJ, 556, 6

This paper has been typeset from a TEX/LATEX file prepared by the author.